Statistical study of seismic heterogeneities at the base of the mantle from PKP differential traveltimes

Raphaël F. Garcia, Sébastien Chevrot and Marie Calvet

Université de Toulouse, Laboratoire de Dynamique Terrestre et Planétaire, UMR5562 *CNRS-INSU, Observatoire Midi-Pyrénées,* 14 *Ave E. Belin,* 31400 *Toulouse, France. E-mail: garcia@dtp.obs-mip.fr*

SUMMARY

Stochastic tomography can provide crucial information on the small-scale structures at the base of the mantle that are still beyond the reach of deterministic imaging. For this purpose, we relate differential traveltime variances of core phases to the correlation function of velocity heterogeneities at the base of the mantle. A global data set of *PKP* traveltimes is then used to invert for statistical properties of velocity perturbations in the D″ layer. We find that the average thickness of D″ is 350 ± 50 km with 1.2 ± 0.3 per cent rms velocity perturbations. The horizontal correlation length is 3° ± 1° and the vertical correlation length 150 ± 75 km. The statistical analysis of the traveltimes of core phases reveals a much stronger energy at short wavelengths compared to global tomographic models, which is in good agreement with the results of most studies of the seismic wavefield scattered at the base of the mantle, based upon the analysis of *PKP* precursors.

Key words: Probability distributions; Mantle processes; Body waves; Seismic tomography; Statistical seismology.

GJI Seismology

1 INTRODUCTION

While the long-wavelength structures in the lower mantle have long been known (Dziewonski *et al.* 1977), the resolution in global tomographic models, despite tremendous and continuous improvements during the last decades, is still limited to about ∼1000 km. The current view of the lower mantle is dominated by two broad regions with lower than average seismic velocities and sharp boundaries, beneath the Pacific and Africa. The stability of these large structures over long periods of time requires higher than average densities relative to surrounding mantle (Le Bars & Davaille 2004). Hotspots seem to be preferentially located along the boundaries of the African and Pacific superswells, where the shear-velocity gradients in tomographic models are the strongest (Thorne & Garnero 2004). Therefore, long wavelength structures imaged at the base of the mantle suggest the presence of both thermal and chemical heterogeneities. The recently discovered phase transformation of perovskite to postperovskite near 120 GPa (Murakami *et al.* 2004) resulted in a profound revolution in our understanding of the D″ layer and offered a simple explanation for the existence of the D″ discontinuity (Lay & Helmberger 1983) which remained a puzzle for geophysicists. Other puzzling observations are the so-called ultralow velocity zones (ULVZ) in which *P* and *S* velocities are reduced by up to 10 and 30 per cent, respectively, which have been imaged in several places on top of the CMB (Thorne & Garnero 2004). The different mechanisms that have been proposed to produce the ULVZs are partial melt (Williams & Garnero 1996), chemical reaction with the liquid outer core (Knittle & Jeanloz 1991) and sedimentation of light materials underside the CMB (Buffett *et al.*

2000). Labrosse *et al.* (2007) have recently proposed that the ULVZ regions are the remnants of the primitive magma ocean that would have sedimented through the mantle and accumulated on top of the CMB. So there is now growing evidence that the base of the mantle is complex, with a significant level of heterogeneity beyond the resolution limit of current tomographic models. Constraining these small-scale structures is important because it is key to understanding the nature and structure of the D″ layer and its role in the global dynamics of the mantle. While the introduction of finite-frequency effects in seismic tomography (Montelli *et al.* 2004) has generated great hopes and fueled many efforts to improve the resolution of tomographic models, the results obtained so far remain disappointing, owing to the poor quality of available global traveltime data sets and to the coarse parametrization used in global tomography.

Statistical analysis of traveltime data can potentially provide important constraints on the distribution of seismic heterogeneities, in particular in the short wavelength limit that is still beyond the reach of deterministic imaging. The idea of statistical or stochastic tomography is not new. For example, from the variances of traveltimes residuals in the ISC data, Gudmundsson *et al.* (1990) inverted the correlation function of seismic velocity heterogeneities and its depth variations. They found a very small level of heterogeneity in the lower mantle, about 0.1 per cent, at a characteristic scale of about 1000 km. On the other hand, they found a stronger heterogeneity in the D″ layer, with velocity variations of 0.3 per cent and a correlation length of 350 km. Other interesting information comes from the analysis of *PKP* precursors which arrive in a time window where direct waves are absent. This provides a unique opportunity to characterize scatterers in the deep Earth. Some of

the older studies suggested that the whole mantle contributes to scattering (Doornbos & Vlaar 1973) while others favoured the D″ region (Haddon & Cleary 1974). More recent statistical studies of *PKP* precursors seem to agree on the whole mantle hypothesis but proposed very different heterogeneity levels (Hedlin *et al.* 1997; Cormier 1999; Margerin & Nolet 2003). A detailed array analysis of a high quality doublet of earthquakes located the source of scattering at the base of the mantle, around the edges of the subducted slab beneath North America (Cao & Romanowicz 2007). Part of the discrepancies between these studies may result from the fact that the different types of seismic observables are sensitive to different part of Earth's heterospectrum, and from the different scattering theories used to interpret the data. Thus, the distribution and strength of heterogeneities in the mantle remains controversial.

In this study, we use a global data set of *PKP* traveltimes obtained by a non-linear waveform inversion of seismological records (Garcia *et al.* 2006). Differential traveltimes of *PKP* waves have a strong sensitivity to velocity heterogeneities at the base of the mantle (Bréger *et al.* 1999; Tkalčić *et al.* 2002). However, the uneven coverage of the base of the mantle obtained by considering *PKP* waves only, combined to the ambiguity between source and receiver legs, preclude a direct tomographic inversion. On the other hand, since differential *PKP* traveltimes sample D″ layer in a wide range of scales, they can be used to constrain the correlation function or the spectrum of seismic heterogeneities. We first formulate an inverse problem, which relates linearly the variances of differential traveltimes of core phases to the correlation function of seismic velocity perturbations. By introducing a simplified description of the correlation function, the number of free parameters can be strongly reduced. Indeed, the statistical description of D″ heterogeneity only involves five parameters: the D″ thickness and heterogeneity level, the horizontal and vertical correlation lengths, and a Hurst coefficient which describes the shape of the correlation function. However, owing to the proximity of the paths above D″, we can only constrain the heterogeneity level in the lower mantle. The thickness, horizontal correlation length and heterogeneity level of the D″ layer are all very well constrained at about 350 km, 3° and 1.2 per cent, respectively, in rather good agreement with previous studies. The other parameters are poorly constrained, but our data suggest a rather small heterogeneity in the lower mantle, about one order of magnitude smaller than in the D″ layer.

2 THEORETICAL BACKGROUND

2.1 General formulation

Fréchet kernels allow us to relate traveltime residuals of core phases to seismic velocity perturbations inside the Earth

$$\delta t_i^j = \int_{V_E} K(p_i)^j(\mathbf{r}) \frac{\delta V}{V}(\mathbf{r}) \mathbf{dr}. \tag{1}$$

In this expression, δt_i^j is the traveltime residual of core phase i (we consider the three *PKP* branches: PKPab, PKPbc and PKPdf) for source–receiver path j, relative to a reference earth model. The vector $\mathbf{r}$ indicates the position inside the Earth (vectors are noted in bold), $K(p_i)^j(\mathbf{r})$ is the sensitivity kernel of phase i and ray parameter p_i, $\frac{\delta V}{V}(\mathbf{r})$ is the velocity perturbation and the integral (1) is taken over the whole volume of the Earth V_E.

From (1), we deduce the expression for the differential traveltime between two core phases (1 and 2) with the same source–receiver geometry j

$$\delta t_1^j - \delta t_2^j = \int_{V_E} \left[K(p_1)^j(\mathbf{r}) - K(p_2)^j(\mathbf{r}) \right] \frac{\delta V}{V}(\mathbf{r}) \mathbf{dr}$$

$$= \int_{V_E} K_d^j(p_1, p_2, \mathbf{r}) \frac{\delta V}{V}(\mathbf{r}) \mathbf{dr}, \tag{2}$$

where $K_d^j(p_1, p_2, \mathbf{r}) = K(p_1)^j(\mathbf{r}) - K(p_2)^j(\mathbf{r})$ is the sensitivity kernel for the differential traveltime. Using a global data set of *PKP* differential travel times, we can compute $\langle (\delta t_1 - \delta t_2)^2 \rangle$ for different epicentral distances, corresponding to various values of parameters p_1 and p_2. This quantity is the differential traveltime variance if the average differential traveltimes are zero. By using eq. (2), and under the hypothesis that the kernels $K_d^j(p_1, p_2, \mathbf{r})$ and velocity perturbations $\frac{\delta V}{V}(\mathbf{r})$ are uncorrelated zero mean functions, we obtain

$$\left\langle (\delta t_1^j - \delta t_2^j)^2 \right\rangle = \left\langle \left(\int_{V_E} K_d^j(p_1, p_2, \mathbf{r}) \frac{\delta V}{V}(\mathbf{r}) \mathbf{dr} \right)^2 \right\rangle$$

$$= \int_{V_E} \int_{V_E} K_d(p_1, p_2, \mathbf{r}_1) K_d(p_1, p_2, \mathbf{r}_2)$$

$$\times \left\langle \frac{\delta V}{V}(\mathbf{r}_1) \frac{\delta V}{V}(\mathbf{r}_2) \right\rangle \mathbf{dr}_1 \mathbf{dr}_2. \tag{3}$$

The cross-product $K_d(p_1, p_2, \mathbf{r}_1) K_d(p_1, p_2, \mathbf{r}_2)$ is the autocorrelation function of differential sensitivity kernels. It can be taken out of the statistical average because it is constant for given values of ray parameters p_1 and p_2, or for given source and receiver positions. Therefore, if the function inside the integral (3) is rotated in the source–receiver reference frame before computing the statistical average, the autocorrelation function of differential kernels is the same for all differential traveltimes corresponding to the same couple of ray parameters (p_1, p_2).

At this point, the hypothesis of statistical independence between differential traveltime sensitivity kernels and velocity perturbations should be discussed, because the uneven data coverage can create spurious correlations between kernels and heterogeneities. Indeed, earthquakes most frequently occur in the Pacific ring subduction zones, and are recorded by stations on continents. Consequently, correlation between sampled heterogeneities and sensitivity kernels is likely to occur, in particular in the source and receiver regions. However, the differential traveltime sensitivity kernels have very small amplitudes close to the source and receiver, and the contribution of these regions to the correlation is negligible. In any case, care must be taken to ensure the best possible homogeneous data distribution before statistical averaging.

By using the autocorrelation functions of the differential kernels

$$A_K(p_1, p_2, \mathbf{r}, \Delta\mathbf{r}) = K_d(p_1, p_2, \mathbf{r}) K_d(p_1, p_2, \mathbf{r} + \Delta\mathbf{r}) \tag{4}$$

and of the velocity perturbations

$$C(\mathbf{r}, \Delta\mathbf{r}) = \left\langle \frac{\delta V}{V}(\mathbf{r}) \frac{\delta V}{V}(\mathbf{r} + \Delta\mathbf{r}) \right\rangle, \tag{5}$$

we obtain the following expression:

$$\left\langle (\delta t_1 - \delta t_2)^2 \right\rangle = \int_{V_E} \int_{\Delta V_E} A_K(p_1, p_2, \mathbf{r}, \Delta\mathbf{r}) C(\mathbf{r}, \Delta\mathbf{r}) \mathbf{dr} \mathbf{d}\Delta\mathbf{r}, \tag{6}$$

where ΔV_E is the whole volume of the Earth covered by the vector variable $\Delta\mathbf{r}$. This integral equation relates linearly the variances of differential traveltime residuals to the autocorrelation function of traveltime heterogeneities through known autocorrelations of the differential traveltime sensitivity kernels. Therefore, by using

different couples of ray parameters (p_1, p_2) one can formulate an inverse linear problem and find the correlation function of velocity perturbations.

2.2 Ray theory framework

Computation of finite frequency sensitivity kernels of *PKP* core phases for dominant periods of the order of 1 s is difficult owing to the B caustic and to the diffractions at the base of the mantle and at the inner core boundary, close to points A and C (Calvet & Chevrot 2005). Therefore, we will hereafter simplify the problem and compute the traveltime kernels with ray theory (at infinite frequency). In that case, traveltimes residuals are only sensitive to structures along the ray path, and the sensitivity kernels are defined by

$$K(p_i)^j(\mathbf{r}) = -\frac{\eta^2}{r\sqrt{\eta^2 - p_i^2}} \frac{\delta[\theta - \theta^j(r)]\delta[\phi - \phi^j(r)]}{r^2 \sin(\theta)}, \qquad (7)$$

where $\eta = \eta(r) = \frac{r}{V(r)}$ is the local slowness, $\delta(x)$ the Dirac delta function and $\theta^j(r)$ and $\phi^j(r)$ the angular positions along the ray as a function of radius r.

To further simplify eq. (7), we assume that the correlation of velocity perturbations depends only on the distance between points $\mathbf{r}_1$ and $\mathbf{r}_2$, varies with radius r only, and is isotropic in the radial and lateral directions. Under these hypotheses, the correlation function can be written as

$$C(\mathbf{r}, \Delta\mathbf{r}) = C(r, \Delta r, \Delta\Phi), \qquad (8)$$

where Δr and $\Delta\Phi$ are the radial and angular distances between points $\mathbf{r}_1$ and $\mathbf{r}_2$, respectively.

By using eqs (8) and (9), and after straightforward algebra, we can rewrite eq. (7) as

$$\left\langle (\delta t_1 - \delta t_2)^2 \right\rangle = \int_{r_{CMB}}^{r_0} \int_{r_{CMB}-r}^{r_0-r} \int_0^\pi R_K(p_1, p_2, r, \Delta r, \Delta\Phi)$$
$$\times C(r, \Delta r, \Delta\Phi) dr d\Delta r d\Delta\Phi, \qquad (9)$$

where r_{CMB} and r_0 are, respectively, the radii of the core–mantle boundary (CMB) and of the Earth's surface. Owing to the Dirac delta distributions, the autocorrelation of the differential traveltime sensitivity kernel $R_K(p_1, p_2, r, \Delta r, \Delta\Phi)$ is non-zero only on four surfaces in the (r, Δr, $\Delta\Phi$) space corresponding to autocorrelations of kernels $K(p_1)(\mathbf{r})$ and $K(p_2)(\mathbf{r})$ (two surfaces), and cross-correlations of kernels $K(p_1)(\mathbf{r})$ and $K(p_2)(\mathbf{r})$, and $K(p_2)(\mathbf{r})$ and $K(p_1)(\mathbf{r})$ (two other surfaces). These functions are defined by

(i) $RK_{11}(p_1, p_2, r, \Delta r, \Delta\Phi) = \frac{\eta^2(r)}{r\sqrt{\eta^2(r)-p_1^2}} \frac{\eta^2(r+\Delta r)}{(r+\Delta r)\sqrt{\eta^2(r+\Delta r)-p_1^2}}$ $\delta[\Delta\Phi - \Delta\Phi_{11}(r, \Delta r)]$ if a point on ray 1 is distant by [Δr, $\Delta\Phi_{11}(r, \Delta r)$] from the point on ray 1 at radius r, and zero elsewhere.

(ii) $RK_{22}(p_1, p_2, r, \Delta r, \Delta\Phi) = \frac{\eta^2(r)}{r\sqrt{\eta^2(r)-p_2^2}} \frac{\eta^2(r+\Delta r)}{(r+\Delta r)\sqrt{\eta^2(r+\Delta r)-p_2^2}}$ $\delta[\Delta\Phi - \Delta\Phi_{22}(r, \Delta r)]$ if a point on ray 2 is distant by [Δr, $\Delta\Phi_{22}(r, \Delta r)$] from the point on ray 2 at radius r, and zero elsewhere.

(iii) $RK_{12}(p_1, p_2, r, \Delta r, \Delta\Phi) = -\frac{\eta^2(r)}{r\sqrt{\eta^2(r)-p_1^2}} \frac{\eta^2(r+\Delta r)}{(r+\Delta r)\sqrt{\eta^2(r+\Delta r)-p_2^2}}$ $\delta[\Delta\Phi - \Delta\Phi_{12}(r, \Delta r)]$ if a point on ray 2 is distant by [Δr, $\Delta\Phi_{12}(r, \Delta r)$] from the point on ray 1 at radius r, and zero elsewhere.

(iv) $RK_{21}(p_1, p_2, r, \Delta r, \Delta\Phi) = -\frac{\eta^2(r)}{r\sqrt{\eta^2(r)-p_2^2}} \frac{\eta^2(r+\Delta r)}{(r+\Delta r)\sqrt{\eta^2(r+\Delta r)-p_1^2}}$ $\delta[\Delta\Phi - \Delta\Phi_{21}(r, \Delta r)]$ if a point on ray 1 is distant by [Δr, $\Delta\Phi_{21}(r, \Delta r)$] from the point on ray 2 at radius r, and zero elsewhere.

So, $R_K = RK_{11} + RK_{22} + RK_{12} + RK_{21}$, and, at a given radius r, this function is non-zero only along four curves in the (Δr, $\Delta\Phi$)

plane. Examples of these curves are shown in Fig. 1 for PKP(BC-DF) traveltime residual at 150° epicentral distance, and at 2740 and 660 km depths. The autocorrelation functions RK_{11} and RK_{22} have positive contributions centred on the origin, whereas cross-correlation functions RK_{12} and RK_{21} have negative contributions centred on the theoretical distance between the two rays at that depth. If the distance between the two rays at a certain depth r_0 is smaller than the correlation length of $C(r_0, \Delta r, \Delta\Phi)$, the velocity heterogeneities are completely correlated, and their contribution to eq. (9) cancels out by summation of positive and negative parts of RK. The examples shown in Fig. 1 demonstrate that PKP(BC-DF) differential traveltimes have a low sensitivity to upper-mantle heterogeneities if the correlation length is larger than 100 km in this part of the mantle. This figure also demonstrates that core phases have a low sensitivity to the radial dependence of the correlation function $C(r, \Delta r, \Delta\Phi)$, because the almost vertical ray paths imply that the sum of the functions RK_{ij} at a given value of Δr almost cancels out.

2.3 Constraints on the correlation function

In order to simplify (6) into (9), we assumed that the correlation function varies only with radius r and distance between the two points, and that it is isotropic in the lateral and radial directions. In addition to these constraints, the correlation function is positive definite. However, because the velocity perturbations have a zero mean on the sphere, the correlation function must have a null zero-order spherical harmonic coefficient (Müller *et al.* 1992; Röhm 1999). As a result, the correlation function on a finite volume (the sphere) is only semi positive definite. Consequently, the zero order spherical harmonic coefficient is zero, and all remaining spherical harmonic coefficients are strictly positive.

In order to invert eq. (9) for the lateral correlation function of velocity perturbations, we introduce an analytic expression of the correlation function, involving a limited number of free parameters. We use Von Karman's correlation functions (Becker *et al.* 2007)

$$\rho_{\lambda,\nu}(x) = 2^{(1-\nu)}(x/\lambda)^\nu \frac{K_\nu(x/\lambda)}{\Gamma(\nu)}, \qquad (10)$$

where x is the cartesian distance between two points, λ the correlation length, $\nu \in [0, 1]$ the Hurst coefficient controlling the shape of the function, K_ν the modified Bessel function of second kind and rational order ν and Γ the gamma function. Replacing the cartesian distance x by the cordal distance $2\sin(\frac{\Delta\Phi}{2})$, where $\Delta\Phi$ is the angular distance, and the correlation length λ by its cordal counterpart $2\sin(\frac{\Lambda}{2})$, we obtain a positive definite correlation function on the sphere (Weber & Talkner 1993; Gaspari & Cohn 1999)

$$\varrho_{\Lambda,\nu}(\Delta\Phi) = \rho_{2\sin(\frac{\Lambda}{2}),\nu}\left(2\sin\frac{\Delta\Phi}{2}\right). \qquad (11)$$

In order to fulfil the null zero-order spherical harmonic coefficient constraint, this function is projected into the space of null zero-order coefficient functions and scaled to unity at the origin in order to insure perfect correlation at zero angular distance

$$\Omega_{\Lambda,\nu}(\Delta\Phi) = \frac{\varrho_{\Lambda,\nu}(\Delta\Phi) - \alpha I}{1 - \alpha}. \qquad (12)$$

In this expression, I is the constant function on the sphere, and

$$\alpha = (\langle I, \varrho_{\Lambda,\nu}\rangle/\langle I, I\rangle). \qquad (13)$$

RK 150 km above CMB   RK at 660 km depth
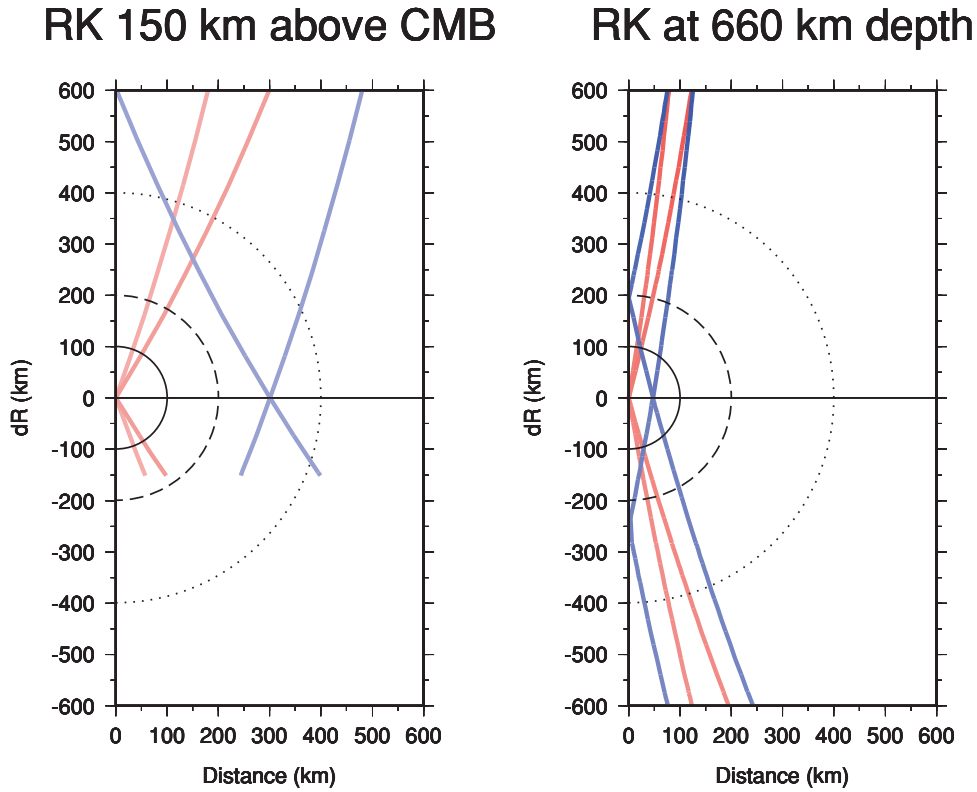
Figure 1. Autocorrelation function $RK(p_1, p_2, r, \Delta r, \Delta\Phi)$ of PKP(BC-DF) traveltime residual kernel at $150°$ epicentral distance, for a source at 256 km depth, plotted at $r = 3631$ km (on the left-hand panel) and at $r = 5711$ km (on the right-hand panel). Colour scale goes from red (positive) to blue (negative), it gives the value of the RK function. The circles centred on the origin simulate a correlation function of velocity heterogeneities with correlation lengths of 100 km (plain line), 200 km (dashed line) and 400 km (dotted line).

Consequently, the function $\Omega_{\Lambda,\nu}(\Delta\Phi)$ is semi-positive definite on the sphere with all spherical harmonic coefficients positive except a null coefficient for order zero.

Owing to the poor sensitivity of core phases differential traveltimes to the radial variations of the correlation function, we assume a simple 1-D exponential correlation function along radial coordinate Δr with a radial correlation length L_c. In order to separate lower-mantle heterogeneities from the ones in D″, the correlation function is written as follows:

(i) $C(r, \Delta r, \Delta\Phi) = \sigma_m^2 e^{-\frac{\Delta r}{L_c}}$ for $r > r_{CMB} + h_{D''}$ (perfect correlation along the horizontal direction in the mantle),

(ii) $C(r, \Delta r, \Delta\Phi) = \sigma_\epsilon^2 e^{-\frac{\Delta r}{L_c}} \Omega_{\Lambda,\nu}(\Delta\Phi)$ for $r_{CMB} < r < r_{CMB} + h_{D''}(\Omega_{\Lambda,\nu}$ angular correlation function in D″ layer) and

(iii) $C(r, \Delta r, \Delta\Phi) = 0$ elsewhere (no effect of core structure, and no radial correlation between D″ layer and the rest of the mantle),

where $C(r, \Delta r, \Delta\Phi)$ is the two point correlation function of velocity heterogeneities, L_c the radial correlation length, σ_m the lower-mantle heterogeneity level, $h_{D''}$ the thickness of D″ layer, Λ, ν and σ_ϵ the correlation length, Hurst coefficient and heterogeneity level inside D″ layer, respectively. Thus, the free parameters are L_c, σ_m, $h_{D''}$, Λ, ν and σ_ϵ. By using these parameters, eq. (9) can be integrated to provide estimates of the traveltime residual variances.

3 DATA SET

The core phase traveltime data are taken from a recently published global study based upon non-linear waveform inversion (Garcia *et al.* 2006), and from traveltime residuals collected by the Interna-

tional Seismological Center (ISC) and reprocessed by Engdahl, van der Hilst and Buland (Engdahl *et al.* 1998) hereafter referred to as EHB. Epicentral distances smaller than $146°$ are excluded to avoid phase misidentifications around the *PKP* triplication. Differential traveltimes involving PKP(BC) and PKP(AB) phases are, respectively, excluded for epicentral distances larger than $152°$ and $166°$, to avoid unmodelled finite frequency diffraction effects at the inner core and core–mantle boundaries. In order to limit the influence of outliers, EHB traveltime residuals with picking errors smaller than 0.01 s and absolute values smaller than 5 s are selected. Similarly, waveform data are selected by imposing traveltime measurement errors smaller than 0.2 s, and correlation coefficients between observed and synthetic seismograms larger than 0.7.

Only PKP(DF) ray paths within $30°$ of equatorial plane are selected to avoid contamination by inner core anisotropy, and traveltimes are corrected for the hemispherical inner core structure with a ±0.2 s correction at epicentral distances smaller than $152°$ (Niu & Wen 2001; Garcia 2002). The selected differential traveltime residuals are plotted as a function of epicentral distance in Fig. 2. In this plot, the differential traveltime variance is varying with core phases and epicentral distance. Differential traveltime variances are computed from summary ray residuals constructed for each event within $2°$ bins in azimuth at the source in order to balance the relative weights between sparse and dense data sampling areas, and to reduce the noise level as much as possible. These summary residuals are then separated in different bins according to the ray parameter of PKPdf phase. The variance within each bin and its related error are computed by a bootstrap method (Efron & Tibshirani 1993). Variance estimates with less than 50 summary ray residuals are
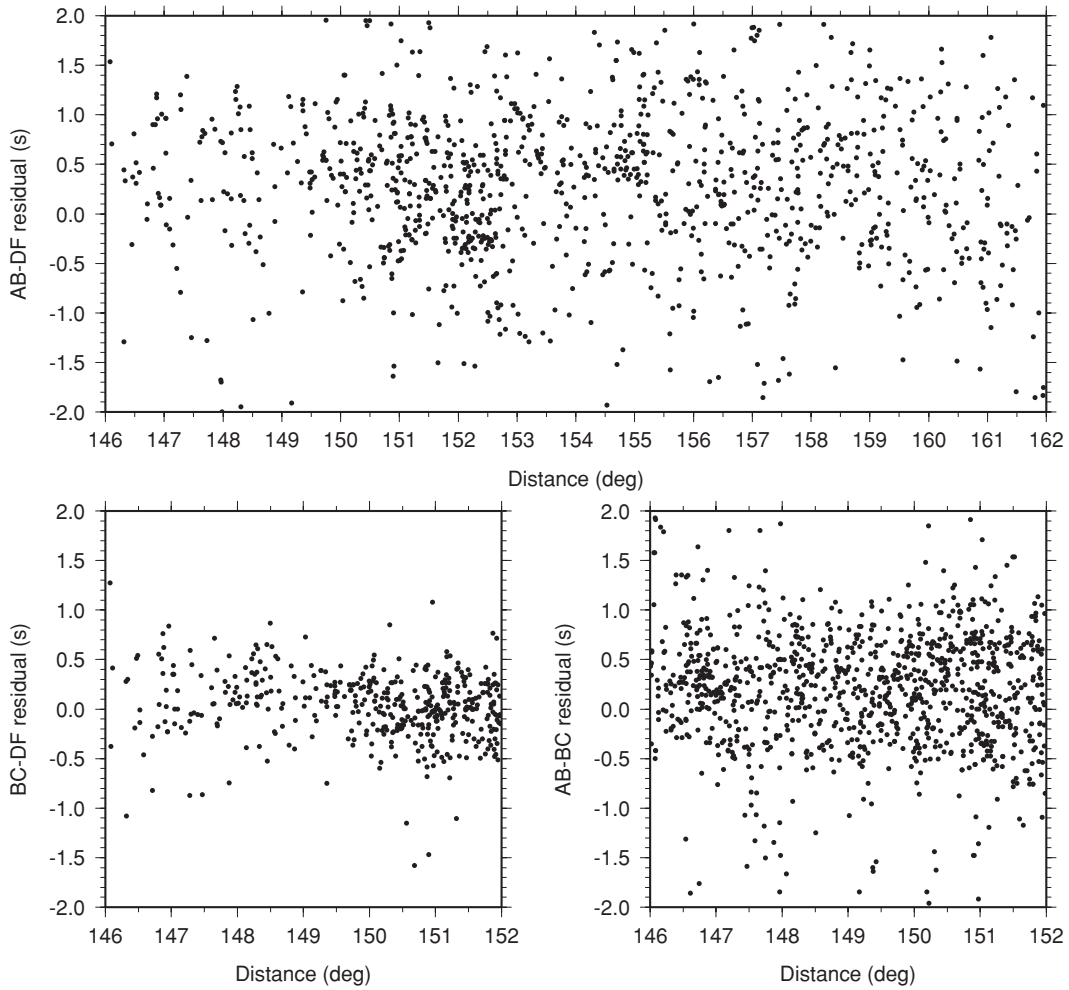
Figure 2. Differential traveltimes residuals of PKP(AB-DF) (top panel), PKP(BC-DF) (bottom left-hand panel), PKP(AB-BC) (bottom right-hand panel) as a function of epicentral distance (in degrees) for the waveform data set of Garcia *et al.* (2006).

excluded. Logarithm of variance as a function of angular distance between two rays at the CMB are plotted in Fig. 3. This distance gives an idea of the sampling of the correlation function along the horizontal direction at the base of the mantle.

Observed differential traveltime variance is given by the sum of noise variance and differential traveltime variance produced by velocity heterogeneities inside the Earth. In order to apply our analysis on differential traveltime variances, Earth's signal must dominate noise. As shown in Fig. 3, the variances obtained from EHB data are five times larger than the ones obtained from our data set which suggests that EHB data are too noisy to be used in the inversion.

At short distances, standard deviations are small because the two phases are very close and sample the same D″ heterogeneities. However, the variance increases with increasing distance to reach a slowly increasing region in which the core phases sample completely uncorrelated heterogeneities. The strong increase of the standard deviation for angular distances around 6° suggests that the correlation length of D″ heterogeneities is close to this value.

4 INVERSION AND RESULTS

The logarithms of differential traveltime variances are inverted by a grid search method over the parameter space. Logarithms are used to insure the positivity of differential traveltime variances. The cost function is defined by

$$\chi^2 = \sum_{i=1}^{N} \frac{\left(LV_d^i - LV_m^i\right)^2}{\sigma_{LV_d^i}^2}, \tag{14}$$

where $N = 13$ is the number of differential traveltime variances, LV_d^i and LV_m^i are, respectively, the observed and modeled logarithms of differential traveltime variances from eq. (9) using the six parameters L_c, σ_m, $h_{D''}$, Λ, ν, σ_ϵ. Parameter $\sigma_{LV_d^i}$ is the error on LV_d^i. The fit obtained with the best model is shown in Fig. 3. The optimal values of the parameters are $\sigma_m = 0$ per cent, $h_{D''} = 400$ km, $\Lambda = 3°$, $\sigma_\epsilon = 1.2$ per cent, $\nu = 0.7$ and $L_c = 150$ km.

The density probability of the parameters is proportional to $e^{-\chi^2/2}$ (Tarantola 1987). The total probability densities of the parameters are plotted in Fig. 4. The Hurst coefficient ν is poorly constrained, but values larger than 0.5 are favoured. Moreover, the model with the lowest cost function is not the one with the highest total probability density, owing to the limitations on the parameter space explored by the grid search method. The lower-mantle heterogeneity level σ_m is close to zero. It is well constrained because the different core phases have different sensitivities to lower-mantle heterogeneities. As a result, even for completely correlated structures along the horizontal direction, the lower-mantle heterogeneities strongly contribute to the differential traveltime variances. The vertical correlation length L_c is better constrained, with a peak probability corresponding to
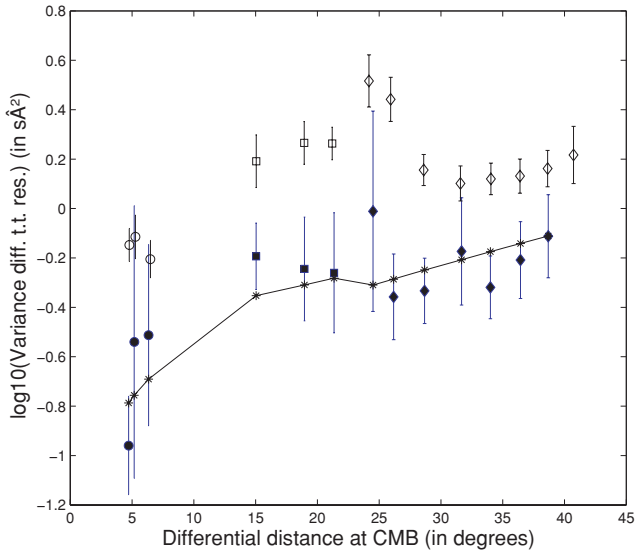
Figure 3. Logarithm of differential traveltime residual variance (in s^2), as a function of differential angular distance (in degrees) between core entry points of the two core phases for different couples of core phases: PKP(BC-DF) (circles), PKP(AB-BC) (squares) and PKP(AB-DF) (diamonds). Open symbols are the variances obtained from ISC data set, and filled symbols are the variances obtained from the PKP waveform data set. The best model fit is plotted with stars and plain line.

150 km. The parameters describing the correlation function of D″ velocity perturbations are rather well constrained. The D″ thickness $h_{D''}$ is found in the range 300–400 km, in good agreement with previous estimates. The correlation length in the D″ layer lies between 2° and 4°. Such a small correlation length reveals the presence of small-scale heterogeneities at the base of the mantle, which are still beyond the resolution of global tomographic studies. The heterogeneity level in D″ layer is found between 1 and 1.5 per cent

rms. These values are consistent with a previous investigation based upon a statistical analysis of *P*-wave traveltimes (Röhm 1999).

Fig. 5 presents the marginal probability densities between couples of parameters. In these plots, the Hurst coefficient is correlated to the horizontal correlation length in D″. Since the shape of the correlation function can be modified by changing either of these parameters, this is not surprising. However most probable horizontal correlation lengths are always smaller than 4°. The D″ heterogeneity level is correlated to D″ thickness because a thick layer of weak heterogeneities can be replaced by a thin layer with strong heterogeneities. However, this correlation is moderate, and optimal values are well constrained. Finally, no correlation is observed between D″ correlation length and D″ heterogeneity level, nor between the vertical correlation length and both the mantle and D″ heterogeneity levels.

To summarize, our results strongly argue in favour of a 350 km thick D″ layer with a high level of small-scale heterogeneities. In the next section, we will compare our results with those inferred from deterministic tomographic imaging of the lower mantle and from studies of seismic waves scattered in the lower mantle, based upon the analysis of *PKP* precursors.

5 COMPARISON WITH PREVIOUS RESULTS

Figs 6(A) and (B) present a comparison between the correlation and covariance functions in different *P*-wave tomographic models taken at the base of the mantle (Inoue *et al.* 1990; Bijwaard *et al.* 1998; Kárason & Van der Hilst 2001; Li *et al.* 2008), and the ones obtained in this study. The rms heterogeneity level of tomographic models is more than one order of magnitude smaller than the estimate obtained from statistical analysis of *PKP* differential times. Moreover, the comparison clearly demonstrates that the short wavelengths evidenced by our statistical analysis are not present in the tomographic models. For models parametrized with spherical harmonics (Inoue
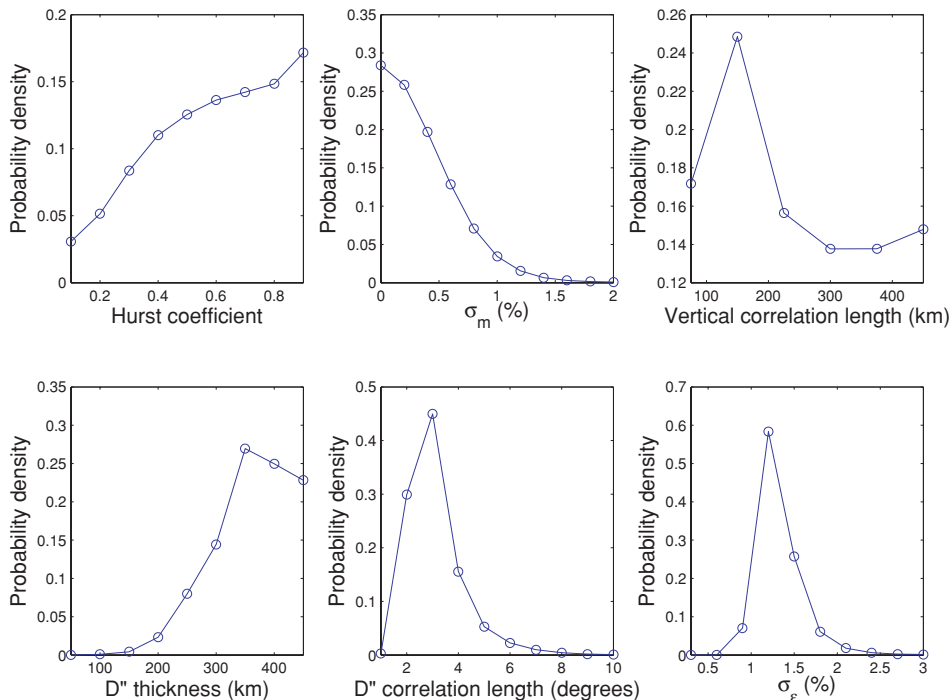
Figure 4. Total probability densities of the six parameters obtained by a grid search over the parameter space.
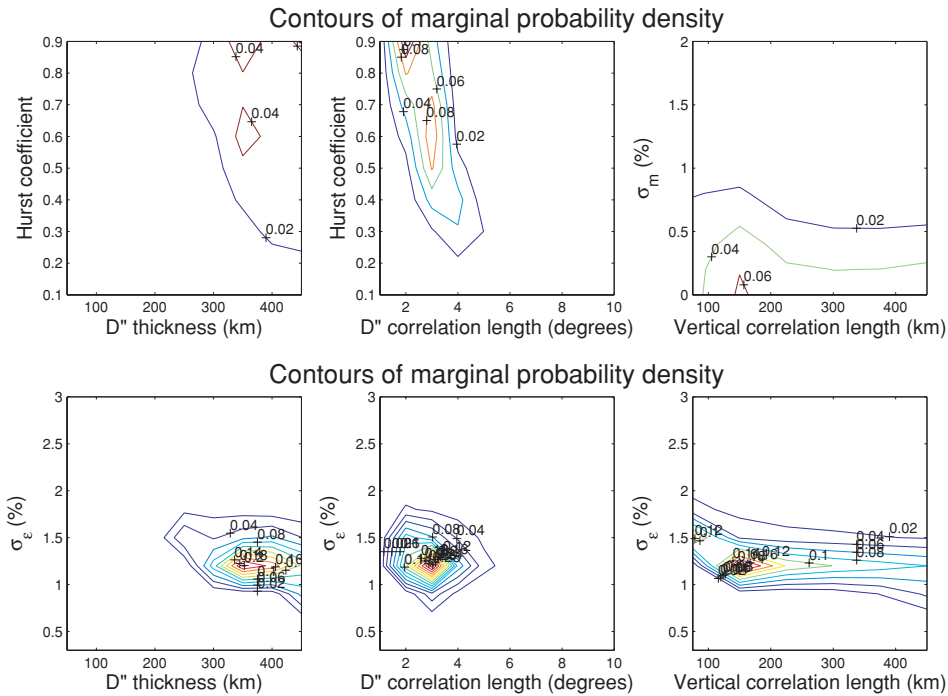
Figure 5. Contours of the marginal probability densities for different couples of parameters.

et al. 1990), the absence of short wavelengths is simply a consequence of truncation of the spherical harmonics expansion at low angular order. However, tomographic models parametrized with blocks of constant velocities (Bijwaard *et al.* 1998; Kárason & Van der Hilst 2001; Li *et al.* 2008) are also characterized by correlation lengths larger than the ones obtained in our statistical analysis. This can be explained by the uneven coverage and high noise level in traveltime data that impose to use a strong smoothing and damping to regularize the inversion.

In Fig. 6(C), we show a comparison in the spectral domain, in which we have included the results of the studies of *PKP* precursors (Bataille & Flatte 1988; Cormier 1999; Margerin & Nolet 2003). The spectra are computed from spherical harmonic expansions of the covariance functions according to the definitions given by Chevrot *et al.* (1998). The analytic expressions of covariance functions (Cormier 1999; Margerin & Nolet 2003) are first transformed to semi-positive definite covariance functions on the sphere, according to eqs (10)–(12). The tomographic models are assumed to be valid in the angular order range 2–20 (wavelength range 8750–1065 km), our statistical analysis in the angular order range 9–60 (wavelength range 2300–360 km), and *PKP* precursors studies in the wavelength range 15–80 km. The spectra of the tomographic models have a k^{-3} power law decrease at the lower limit of the spectrum in the upper mantle (Chevrot *et al.* 1998), whereas our statistical analysis favours a slope of −2.5. If we compare the spectra in the wavelength domain where their validity overlap, the slopes are different by a factor of two. This difference suggests that the regularization constraints imposed in tomographic inversions strongly filter out the short wavelengths of velocity perturbations. From *PKP* precursors scattered at the base of the mantle, Bataille & Flatté (1988) found a power law spectrum with a slope of −5.3, but we have not been able to renormalize their spectrum in a way consistent with our definitions. However, similar studies obtained, respectively, a 1 per cent rms heterogeneity level with a Gaussian correlation function with a 10 km correlation length (Cormier 1999), and a

0.32 per cent rms heterogeneity level with a 'Henyey–Greenstein' (H–G) correlation function with a 30 km correlation length (Margerin & Nolet 2003) in the wavelength range 15–80 km. In the spectral domain, these models correspond to power law decrease with coefficients −2.8 and −2.4, which are consistent with an extrapolation of our spectrum towards shorter wavelengths (Fig. 6C).

6 INFLUENCE OF DISCONTINUITIES TOPOGRAPHY

The traveltimes of refracted core phases are also sensitive to undulations of seismic discontinuities, such as the CMB or the discontinuity at the top of D'' layer. Owing to the strong velocity contrast between iron outer core and silicate mantle, the former can have a significant influence on *PKP* traveltimes. An analysis similar to the one done for velocity heterogeneities can be performed to invert the *PKP* differential travel variances for the correlation function of CMB topography only. This correlation function is defined by:

$$C(\Delta\Phi) = \sigma_h^2 \Omega_{\Lambda_h, \nu}(\Delta\Phi),$$

where $\Delta\Phi$ is the epicentral distance between the two points on the CMB, σ_h the rms topography (in km), Λ_h and ν the correlation length (in degrees) and the Hurst coefficient, respectively. Fig. 7 presents the probability density functions of these three parameters. The optimal values are $\nu = 0.85 \pm 0.15$, $\Lambda_h = 4.5° \pm 0.5°$ and $\sigma_h = 5.2 \pm 0.4$ km. The data fit (not shown) is similar to the one obtained for velocity heterogeneities.

By integrating the corresponding CMB topography spectrum for wavelengths larger than 360 km (6° epicentral distance at the CMB), we obtain a value of 4.33 km rms CMB topography. This result is in contradiction with previous seismological studies (Garcia & Souriau 2000; Sze & van der Hilst 2003) which predict, respectively, values of 2 ± 0.7 and 0.6 km for wavelengths larger than 360 km on the CMB. Consequently, CMB topography alone cannot explain the observed traveltimes residuals of core phases. Moreover, previous
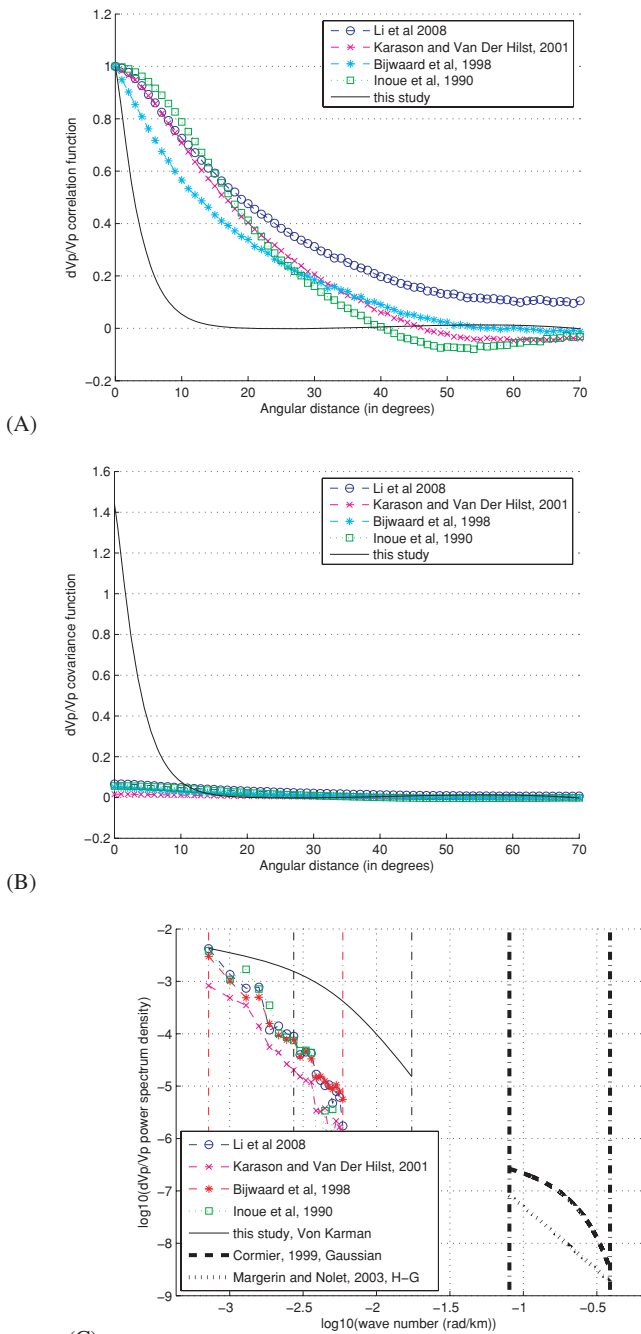
Figure 6. Comparison between correlation functions (A) and covariance functions (B) of D″ velocity perturbations in various tomographic models and our results (plain line). Comparison between the spectra of the tomographic models (colours) and our model (thin black line) and the results of studies of PKP precursors by Cormier (1999) (thick black dashed line) and Margerin and Nolet (2003) (thick black dotted line) (C). Dot–dashed vertical lines represent the wavenumber domain in which the tomographic models (red lines), the statistical analysis (thin black lines) and the study of scattered wavefield (thick black lines) are valid.

investigations of CMB topography for wavelengths larger than 360 km provided by studies of Earth's rotation (Gwinn *et al.* 1986; Herring *et al.* 1986; Hinderer *et al.* 1990; Mathews *et al.* 2002), reflected phases (Garcia & Souriau 2000; Sze & van der Hilst 2003)

and mantle flow modelling (Steinberger & Holme 2008) all predict a small topography which has probably a marginal contribution to our *PKP* traveltimes anomalies.

The transformation of perovskite to post-perovskite is now the favoured explanation for a discontinuity at the top of the D″ layer. Due to the large clapeyron slope of this phase change, the topography of the D″ discontinuity is expected to be quite large, of the order of a few hundred kilometres over scales that are related to the lateral variations of temperature in D″ (Monnereau & Yuen 2007). However, the *P*-wave velocity contrast of this phase transition at constant chemistry is small (Oganov & Ono 2004; Stackhouse *et al.* 2006). Consequently, D″ discontinuity topography is expected to have a small contribution to *P*-wave traveltime anomalies.

To conclude, we are thus inclined to favour the effects of volumetric compressional velocity anomalies produced by lateral variations of temperature and chemistry to explain the observed traveltime anomalies.

7 CONCLUSION

The variances of differential traveltime residuals are linearly related to the correlation function of velocity heterogeneities. Statistical analysis of core phases traveltimes allows us to determine the horizontal structure of the correlation function at the base of the mantle but the radial structure of the correlation function remains poorly constrained. Because noise variance contributes to differential traveltime variances, only high quality differential traveltime data, in which noise variance is small compared to Earth's signal, can be exploited. Our global data set of *PKP* traveltimes (Garcia *et al.* 2006) appears to fullfil this criterion. However, the limited number of distance ranges in which we can compute traveltime variances only allows us to invert for a simplified correlation function. Despite its simplicity, our model statistically explains the observations of *PKP* traveltimes and brings strong constraints on lower-mantle structures. The heterogeneity level of the lower mantle outside D″ layer is close to 0 ± 0.2 per cent rms, and the D″ layer is best described as a 350 ± 50 km thick layer with 1.2 ± 0.3 per cent rms velocity perturbations. The horizontal correlation length is about $3° \pm 1°$, the vertical correlation length 150 ± 75 km, and the Hurst coefficient $\nu = 0.7 \pm 0.2$. The main limitations on these results are coming from the unknown influence of noise on the differential traveltime variances, and from the use of ray theory instead of finite-frequency sensitivity kernels.

The thickness, heterogeneity level, and the small correlation length of velocity heterogeneities inside D″ are all consistent with most models of D″ layer proposed previously. The heterospectrum at the base of the mantle provides important constraints to discriminate numerical models of thermochemical convection (Deschamps & Tackley 2008, 2009). It is interesting to note that the small-scale features obtained in this study are still beyond the resolution limit of seismic tomography, and that the extrapolation of our heterogeneity spectrum towards short wavelengths is consistent with the results of studies of seismic wave scattering at the base of the mantle. Finally, small-scale structures at the base of the mantle produce potentially strong residuals in differential traveltimes of core phases that are classically interpreted in terms of structures in the inner core (Bréger *et al.* 1999). To separate these contributions, lower mantle and inner core structures should be inverted simultaneously in future tomographic studies. Constraining small-scale structures of the D″ layer thus remains an important challenge for seismologists, which will require new, higher quality, global body wave traveltime and amplitude data.
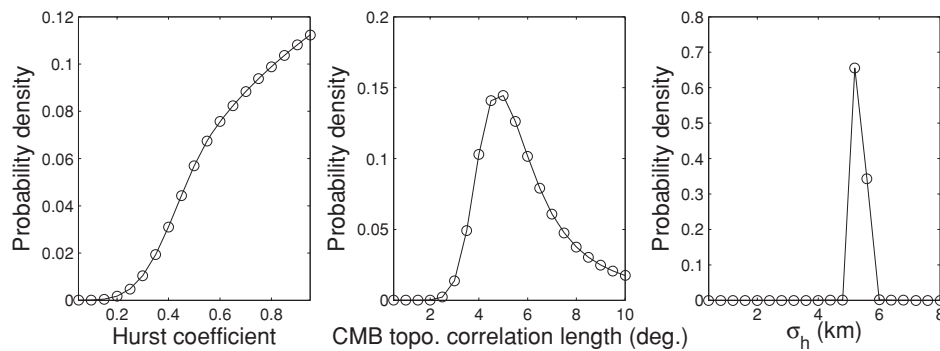
Figure 7. Total probability densities of the three parameters describing the correlation function of core–mantle boundary topography.

REFERENCES

Bataille, K. & Flatte, S.M., 1988. Inhomogeneities near the core-mantle boundary inferred from short-period scattered PKP waves recorded at the global digital seismograph network, *J. geophys. Res.,* **93,** 15 057–15 064.

Becker, T.W., Browaeys, J.T. & Jordan, T.H., 2007. Stochastic analysis of shear-wave splitting length scales, *Earth planet. Sci. Lett.,* **259,** 526–540.

Bijwaard, H., Spakman, W. & Engdahl, E., 1998. Closing the gap between regional and global travel time tomography, *J. geophys. Res.,* **103,** 30 055–30 078.

Bréger, L., Romanowicz, B. & Tkalčić, H., 1999. PKP(BC-DF) travel time residuals and short scale heterogeneity in the deep Earth, *Geophys. Res. Lett.,* **26,** 3169–3172.

Buffett, B.A., Garnero, E.J. & Jeanloz, R., 2000. Sediments at the top of Earth's core, *Science,* **290,** 1338–1342.

Calvet, M. & Chevrot, S., 2005. Traveltime sensitivity kernels for PKP phases in the mantle, *Phys. Earth planet. Inter.,* **153,** 21–31.

Cao, A. & Romanowicz, B., 2007. Locating scatterers in the mantle using array analysis of PKP precursors from an earthquake doublet, *Earth planet. Sci. Lett.,* **255,** 22–31.

Chevrot, S., Montagner, J.P. & Snieder, R., 1998. The spectrum of tomographic earth models, *Geophys. J. Int.,* **133,** 783–788.

Cormier, V.F., 1999. Anisotropy of heterogeneity scale lengths in the lower mantle from PKIKP precursors, *Geophys. J. Int.,* **136,** 373–384.

Deschamps, F. & Tackley, P.J., 2008. Searching for models of thermo-chemical convection that explain probabilistic tomography. I. Principles and influence of rheological parameters, *Phys. Earth planet. Int.,* **171,** 357–373.

Deschamps, F. & Tackley, P.J., 2009. Searching for models of thermo-chemical convection that explain probabilistic tomography. II, *Phys. Earth planet. Int.*, **176,** 1–18.

Doornbos, D. & Vlaar, N., 1973. Regions of seismic wave scattering in the Earth's mantle and precursors to PKP, *Nature,* **243,** 58–61.

Dziewonski, A.M., Hager, B.H. & O'Connell, R.J., 1977. Large-scale heterogeneities in the lower mantle, *J. geophys. Res.,* **82,** 239–255.

Efron, B. & Tibshirani, R., 1993. *An Introduction to the Bootstrap*, Monographs on Statistics and Applied Probability Series, CRC Press, Boca Raton, FL.

Engdahl, E., Van der Hilst, R. & Buland, R., 1998. Global teleseismic earthquake relocation with improved travel times and procedures for depth determination, *Bull. seism. Soc. Am.,* **88,** 722–743.

Garcia, R., 2002. Constraints on upper inner core structure from waveform inversion of core phases, *Geophys. J. Int.,* **150,** 651–664.

Garcia, R. & Souriau, A., 2000. Amplitude of the core-mantle boundary topography estimated by stochastic analysis of core phases, *Phys. Earth planet. Inter.,* **117,** 345–359.

Garcia, R., Tkalčić, H. & Chevrot, S., 2006. A new global PKP data set to study Earth's core and deep mantle, *Phys. Earth planet. Inter.,* **159,** 15–31.

Gaspari, G. & Cohn, S.E., 1999. Construction of correlation functions in two and three dimensions, *Q. J. R. Meteorol. Soc.,* **125,** 723–757.

Gudmundsson, O., Davies, J.H. & Clayton, R.W., 1990. Stochastic analysis of global travel time data, mantle heterogeneity and random errors in the ISC data, *Geophys. J. Int.,* **102,** 25–43.

Gwinn, C., Herring, T. & Shapiro, I., 1986. Geodesy by radio interferometry: Studies of the forced nutations of the Earth 2. interpretation, *J. geophys. Res.,* **91,** 4755–4765.

Haddon, R.A.W. & Cleary, J.R., 1974. Evidence for scattering of seismic PKP waves near the mantle-core boundary, *Phys. Earth planet. Inter.,* **8,** 211–234.

Hedlin, M.A.H., Shearer, P.M. & Earle, P.S., 1997. Seismic evidence for small-scale heterogeneity throughout the Earth's mantle, *Nature,* **387,** 145–150.

Herring, T.A., Gwinn, C.R. & Shapiro, I.I., 1986. Geodesy by radio interferometry: studies of the forced nutations of the earth. I – Data analysis. II – Interpretation, *J. geophys. Res.,* **91,** 4745–4765.

Hinderer, J., Legros, H., Jault, D. & Le Mouël, J.-L., 1990. Core-mantle topographic torque: a spherical harmonic approach and implications for the excitation of the Earth's rotation by core motions, *Phys. Earth planet. Inter.,* **59,** 329–341.

Inoue, H., Fukao, Y., Tanabe, K. & Ogata, Y., 1990. Whole mantle P-wave travel time tomography, *Phys. Earth planet. Inter.,* **59,** 294–328.

Kárason, H. & Van der Hilst, R., 2001. Tomographic imaging of the lower-most mantle with differential times of refracted and diffracted core phases (PKP, Pdiff), *J. geophys. Res.,* **106,** 6569–6587.

Knittle, E. & Jeanloz, R., 1991. Earth's core-mantle boundary: results of experiments at high pressures and temperatures, *Science,* **251,** 1438–1443.

Labrosse, S., Hernlund, J.W. & Coltice, N., 2007. A crystallizing dense magma ocean at the base of the Earth's mantle, *Nature,* **450,** 866–869.

Lay, T. & Helmberger, D., 1983. A shear velocity discontinuity in the lower mantle, *Geophys. Res. Lett.,* **10,** 63–66.

Le Bars, M. & Davaille, A., 2004. Whole layer convection in a heterogeneous planetary mantle, *J. geophys. Res.,* **109,** B03403, doi:1029/2003JB002617.

Li, C., van der Hilst, R.D., Engdahl, E.R. & Burdick, S., 2008. A new global model for P wave speed variations in Earth's mantle, *Geochem., Geophys., Geosyst.,* **9,** Q05018, doi:10.1029/2007GC001806.

Margerin, L. & Nolet, G., 2003. Multiple scattering of high-frequency seismic waves in the deep Earth: PKP precursor analysis and inversion for mantle granularity, *J. geophys. Res.,* **108**(B11), 2514, doi:10.1029/2003JB002455.

Mathews, P.M., Herring, T.A. & Buffett, B.A., 2002. Modeling of nutation and precession: new nutation series for nonrigid Earth and insights into the Earth's interior, *J. geophys. Res.,* **107**(B4), 2068, doi:10.1029/2001JB000390.

Monnereau, M. & Yuen, D.A., 2007. Topology of the postperovskite phase transition and mantle dynamics, *Proc. Natl. Acad. Sci.,* **104,** 9156–9161.

Montelli, R., Nolet, G., Dahlen, F.A., Masters, G., Engdahl, E.R. & Hung, S.-H., 2004. Finite-frequency tomography reveals a variety of plumes in the mantle, *Science,* **303,** 338–343.

Müller, G., Roth, M. & Korn, M., 1992. Seismic-wave traveltimes in random media, *Geophys. J. Int.,* **110,** 29–41.

Murakami, M., Hirose, K., Kawamura, K., Sata, N. & Ohishi, Y., 2004. Post-perovskite phase transition in $MgSiO_3$, *Science,* **304,** 855–858.

Niu, F. & Wen, L., 2001. Hemispherical variations in seismic velocity at the top of the Earth's inner core, *Nature,* **410,** 1081–1084.

Oganov, A.R. & Ono, S., 2004. Theoretical and experimental evidence for a post-perovskite phase of MgSiO3 in Earth's D'' layer, *Nature,* **430,** 445–448.

Röhm, A., 1999. Statistical properties of travel time measurements and the structure of the Earth's mantle, *PhD thesis*, Mededelingen van de Faculteit Aardwetenschappen Universiteit Utrecht.

Stackhouse, S., Brodholt, J.P. & Price, G.D., 2006. Elastic anisotropy of FeSiO3 end-members of the perovskite and post-perovskite phases, *Geophys. Res. Lett.,* **33,** 1304.

Steinberger, B. & Holme, R., 2008. Mantle flow models with core-mantle boundary constraints and chemical heterogeneities in the lowermost mantle, *J. geophys. Res.,* **113,** B05403, doi:10.1029/2007JB005080.

Sze, E.K.M. & van der Hilst, R.D., 2003. Core mantle boundary topography from short period PcP, PKP, and PKKP data, *Phys. Earth planet. Int.,* **135,** 27–46.

Tarantola, A., 1987. *Inverse Problem Theory*, Elsevier Science Publishers, B.V., Amsterdam.

Thorne, M.S. & Garnero, E.J., 2004. Inferences on ultralow-velocity zone structure from a global analysis of SPdKS waves, *J. geophys. Res.,* **109,** B08301, doi:10.1029/2004JB003010.

Tkalčić, H., Romanowicz, B. & Houy, N., 2002. Constraints on D'' structure using PKP(AB-DF), PKP(BC-DF), and PcP-P traveltime data from broadband records, *Geophys. J. Int.,* **148,** 599–616.

Weber, R.O. & Talkner, P., 1993. Some remarks on spatial correlation function models, *Mon. Wea. Rev.,* **121,** 2611–2617.

Williams, Q. & Garnero, E.J., 1996. Seismic evidence for partial melt at the base of Earth's mantle, *Science,* **273,** 1528–1530.